Monte Carlo studies of grain growth on curved surfaces

P. Peczak and Gary S. Grest
Exxon Research and Engineering Company, Corporate Research Science Laboratories, Annandale, New Jersey 08801-0998

Dov Levine
Department of Physics, Technion–Israel Institute of Technology, Haifa 32000, Israel
(Received 10 May 1993)

Monte Carlo simulations have been carried out to study the effect of surface curvature on normal grain growth. As predicted by a recent theory of kinetics of coarsening on curved surfaces, we find that the stability properties of stationary grains are sensitive to the Gaussian curvature of the surface. In particular, it is found that on a spherical surface, the normalized grain-size distribution is not stationary in time. In regions of positive curvature, grains that are much larger than the mean are unstable and grow faster than the mean and engulf the entire surface. In regions of negative curvature, all stationary grains are stable and the final configuration consists of many grains which have established a stable size. These observations are in agreement with results of experimental studies of the growth of grains in polycrystalline films on curved surfaces.

PACS number(s): 82.70.Rr, 68.10.−m

I. INTRODUCTION

During the past several years, there has been a considerable interest in the coarsening dynamics of two-dimensional (2D) cellular patterns [1–3]. An example of cellular structure includes foams, polycrystalline aggregates in metals, ceramics and alloys, biological tissues, magnetic bubbles in garnets, and monolayers of fatty acids on water in their liquid-gas coexistence region. In all such systems the essential mechanism of evolution is intercellular diffusion resulting in reduction of surface energy [2,3]. However, the dynamics of coarsening of 2D cellular patterns still remains somewhat controversial. Despite all the theoretical and computational effort [4–27] directed towards understanding the evolution of statistical properties and the long-time behavior of 2D structures, the exact solution of the model is still not known, particularly in regard to which features are universal and which are system specific.

One of the simplest 2D systems that exhibits all the intrinsic properties of more complex materials with domain structure is a soap froth. The basic mechanism for diffusive coarsening in foams is described by von Neumann's law for the rate of change of the area A_n of an n-sided cell [4]

$$\frac{dA_n}{dt}=\frac{D\sigma\pi}{3}(n-6)\ , \tag{1}$$

where σ is the surface tension and D is the diffusion constant for transport through the bubble wall. This law was originally obtained assuming that the diffusion rate of incompressible gas across the walls is proportional to the pressure difference between the adjacent bubbles, and thus to the curvature of their interfaces. The foam is assumed to be an idealized, 2D system in a state of mechanical equilibrium, with no Plateau borders [28] and all interfaces meeting at angles of 120°. (These conditions are sometimes called Plateau laws.) However, it is now believed that the physics of many 2D patterns is similar and Eq. (1) also applies to a wider class of problem including polycrystalline aggregates in metals [5]. In this case, the diffusion constant D should be replaced by the grain-boundary mobility M.

Recently, a generalization of von Neumann's law was obtained for the coarsening of foams constrained to *curved* surfaces [17,29]. Generalizing the condition for the balance of forces, due to the pressure difference and the surface tension, and assuming that all the edges have constant geodesic curvature, one finds that

$$\frac{dA_n}{dt}=\frac{D\sigma\pi}{3}\left\{(n-6)+\frac{3}{\pi}\int_S K dA\right\}\ . \tag{2}$$

Here the integral of the Gaussian curvature is over the area of the bubble's face S characterized by a Gaussian curvature $K(S)$. For a flat surface $K=0$ and one obtains the standard von Neumann's relation, Eq. (1). The additional term in Eq. (2) is small, of the order of $O(F^{-1})$, where F is the total number of domains on the surface [30]. Nevertheless, the evolution of bubbles on a surface characterized by the Gaussian curvature K should be very different from its planar counterpart. In particular, if $K>0$, no bubble on a positively curved surface is stable, while all stationary bubbles on a surface with $K<0$ are stable [17].

A very useful method of studying a general phenomenon of the kinetics of growth is to develop a coarse-grained model which is not specific to the details of any one system. Among such approaches a microscopic microstructural approach in the form of the two-dimensional Potts model has been demonstrated to be particularly useful [24–27,31–34]. In this model, a cellular aggregate is represented by a lattice of spins. Each grain is characterized by an unique spin or orientation and the interface between regions of different orientations

corresponds to grain boundaries. The Q-state Potts-model Hamiltonian is defined as [35]

$$H_0 = J \sum_{\{ij\}} (1-\delta_{S_i S_j}) , \tag{3}$$

where J is a positive constant proportional to the grain-boundary energy unit, the sum is taken over all appropriate neighbor site pairs $\{ij\}$ with assigned spins (orientations) $1 \le S_i \le Q$, and $\delta_{\alpha\beta}$ is the Kronecker delta function. For the triangular lattice the summation is carried out over all nearest-neighbor pairs $\{ij\}$ while for the square lattice all nearest and next-nearest sites j of site i are included [33]. The number of possible states Q is usually taken large enough to assure that an impingement of different domains with the same orientation is relatively infrequent. The growth process is simulated by random jumps of spins across the interface under constraint of the energy-minimization principle. Dynamic evolution of microstructure proceeds by a curvature driven grain-boundary migration and, on an average, obeys von Neumann's coarsening law [31].

While the patterns formed in soap froth and polycrystalline aggregates are very similar, the dynamics differ in two essential ways. Soap-froth dynamics is relatively slow in comparison to the readjustment of the soap films, being governed by the pressure difference between neighbor bubbles, which allows the cell wall to approach a smooth (minimal) surface [5]. In metallic aggregates, the probabilistic motion of an interface between the domain of different orientation results in grain boundaries which are usually far from these ideal surfaces [32,36]. A second difference between an ideal soap froth and the polycrystalline aggregate is orientational anisotropy of the boundary energy of the latter which may significantly affect the coarsening kinetics [33]. Clearly, the Potts model is closer in detail to the polycrystalline microstructures. Nevertheless, the low-lattice-anisotropy Potts-model simulations show an overall excellent agreement with behavior of a real soap forth [32,33]. This apparent success of the Potts model in describing both systems motivated us to find an extension of the lattice-based Potts model to study the behavior of soap froths on a curved surface.

One method of modeling the effect of the Gaussian curvature $K(S)$ on coarsening dynamics is to introduce an implicit dependence of the Potts Hamiltonian on $K(S)$, e.g., through $H_0 \to H(\{K_j\}_{1 \le j \le N})$, where K_j represents the Gaussian curvature at the jth site of the lattice, $1 \le j \le N$. Moreover, an appropriate contribution to the "flat" Potts Hamiltonian should be consistent with its topological, i.e., global character [37]. By virtue of the Gauss-Bonnet theorem [38], the integral of K over a closed surface depends only on its genus g, $\int_S K dA = 4\pi(1-g)$. Therefore, a reasonable class of modified Potts Hamiltonians, $H(\{K_i\})$ should satisfy the relation, in the absence of any interface (in a one-domain state),

$$H(\{K_i\})|_{\text{no interfaces}} \propto C_0 + C_1(1-g)^1 + C_2(1-g)^2 + \cdots . \tag{4}$$

Clearly, the simplest class of models with this property corresponds to $C_i \equiv 0$, $i = 2, 3, \ldots$, i.e., can be realized by a linear curvature "field" term. Simulations with such a model are presented in this paper.

An alternative method is to introduce dynamical effects related to the Gaussian curvature indirectly, *via* an appropriate lattice formulation of the standard Potts model. Since the surface tension of the soap froth is essentially isotropic even on a curved surface, it is natural to seek a lattice-based formulation of the model with use of a *regular* tessellation of a surface [39]. However, many recent studies have demonstrated that the level of anisotropy in a Potts Hamiltonian has an influence on the kinetics of coarsening [33,40]. In some cases, the strong anisotropy of the lattice can lead to pinning at low temperatures and qualitative differences in the results for a number of topological distribution functions. The study with use of this method, applied to coarsening on a surface with negative, constant curvature, i.e., pseudosphere, is presented in Sec. V.

II. THE MODIFIED POTTS MODEL

The Hamiltonian of the modified Q-state Potts model with a linear Gaussian curvature term can be defined by

$$H = H_0 + H_K = J \sum_{\{ij\}} (1-\delta_{S_i S_j}) - c \sum_i \left[\sum_j K_j \delta_{S_i S_j} \right] , \tag{5}$$

where the first is the same as Eq. (3) and c is a constant. Both summations in H_K are carried out over all lattice sites and K_j is the local Gaussian curvature of a surface element at site j. The fieldlike term $\kappa_i \equiv -\sum_j K_i \delta_{S_j S_i}$ represents a sum of Gaussian curvature increments over all sites j of a domain with orientation $S_j = S_i$. Since the local Gaussian curvature K_i is inversely proportional to the total number of sites N, H_K is an intensive variable, i.e., $H_K \propto N$. Indeed, if the surface is occupied by just one grain, the total energy per site is

$$\frac{H}{N} = -c \sum_j \kappa_j \to -c \int_S K \, dA \propto (g-1) ,$$

which correctly accounts for the genus of a surface. It is worth noting that if the whole surface is occupied by just two domains with orientations S_1 and S_2, each site of domain 1, 2 contributes a field term $\kappa_1 \equiv \sum_p^{(1)} K_p$, $\kappa_2 \equiv \sum_r^{(2)} K_r$, respectively. The total contribution of the Gaussian curvature to the Hamiltonian is, therefore, $-c(N_1\kappa_1 + N_2\kappa_2)$, where N_i is total number of sites in domain i. In the special case, when $K_j \equiv K = \text{const}$, e.g., for a spherical surface, the sum reduces to $-cK(N_1^2 + N_2^2)$. Generally, if there are $s > 2$ domains covering the surface with $K = \text{const}$, then $-H_K = cK(N_1^2 + N_2^2 + \cdots + N_s^2)$. Since

$$\sum_{i=1}^{s} N_i^2 \le \left[\sum_{i=1}^{s} N_i \right]^2 = N^2 ,$$

on a surface of a sphere ($K > 0$) the configuration with the lowest value of H_K corresponds to one domain with

sites, whereas on a surface with negative curvature, the minimum of H_K is achieved when the configuration consists of N one-site cells. Hence, the curvature part of Eq. (5) leads to ground states which are consistent with the dynamics described by the modified von Neumann's equation, Eq. (2).

It should be observed that this method of representing dynamic effects, due to the Gaussian curvature, by a fieldlike term requires the use of reasonably large lattices. In particular, the area of a typical domain should be much smaller than the inverse of the mean Gaussian curvature of the grain, i.e., $(A/L^2) \ll \bar{K}^{-1}$. Otherwise, local variations in K averaged over an area will not capture the correct dynamic behavior of the froth.

The kinetics of the interface is simulated by the finite-temperature Metropolis Monte Carlo method with the Glauber excitation mechanism. After a site is selected at random, a new orientation is randomly chosen, and the change in energy $\Delta E = H_{\rm fin} - H_{\rm in}$ associated with this change is evaluated. The reorientation is accepted with probability $\min\{1;\exp(-\Delta E/k_B T)\}$. In particular, if a site i of a domain α attempts to change its orientation to that of an adjacent domain β, then

$$-\Delta E = -\Delta E_0 + c[\kappa_\alpha + K_i(N_\alpha + 1)] - c[\kappa_\beta + K_i(N_\beta - 1)], \tag{6}$$

where ΔE_0 is the change in energy due to H_0, Eq. (3). For a spherical surface $K = \text{const}$, the energy cost of flipping a spin from orientation α to β is $\Delta E = \Delta E_0 - 2cK(N_\alpha - N_\beta)$. Therefore, the rate change in the area of a domain α includes a term which is consistent with the Gaussian curvature term in the modified von Neumann's law, Eq. (3). Moreover, the probability of a spin flip $S_\beta \to S_\alpha$ of an interface site belonging to a domain β is normalized by a factor which assures that, if domains α and β are of comparable size, $N_\alpha \cong N_\beta$, the system is in a state of unstable equilibrium.

In the present study, we kept the maximum number of accessible domain orientations constant, $Q = 48$, and kept a separate count of all grains. Because each grain does not have a unique orientation, this occasionally leads to impingement of grains with the same orientation. Every 20–100 Monte Carlo steps per site (MCS), we checked whether such an impingement had occurred. If so, then a new grain of size equal to the sum of adjacent grains with the same orientation was identified, with the appropriate field term for the new grain. While this impingement sometimes leads to abrupt changes in the local grain size, it did not significantly influence our final results [41]. For both cases of spherical and toroidal surfaces, typically five different Monte Carlo runs with up to 1.0×10^5 MCS were used to obtain averages. Initial configurations were obtained from a completely disordered state by normal growth [24]. This yielded microstructures with an initial mean grain size of $A_0 \cong 14$, with a standard deviation of 10. Simulations were performed at $T = 0.171J$, which is about $0.231 T_c^\Delta$, where T_c^Δ is the critical temperature for the triangular lattice [42]. Since both lattices were relatively large, $N \geq 4 \times 10^5$, and their local symmetry almost everywhere was that of a triangular lattice, one can expect that in both cases the transition temperatures were not too far from T_c^Δ (Ref. [43]). It is worth noting that the finite-temperature simulations were necessary in order to overcome local frustration of the driving force which can pin the growth at $T = 0$ (Ref. [40]). In the following section we give a detailed account of finite-temperature quenching studies for the modified Potts model on a sphere and torus.

III. RESULTS FOR SPHERICAL SURFACE

The simplest system with only a constant, positive Gaussian curvature is the surface of a sphere. In this case we used a mesh obtained by a spherical projection of triangularly tessellated icosahedron [44]. The starting point of this construction is provided by the 12 vertices of an icosahedron. The coordinates of these vertices are taken as $(0, \pm 1, \pm\tau)$, $(\pm 1, \pm\tau, 0)$ and $(\pm\tau, 0, \pm 1)$ where τ is the Golden ratio $(1+\sqrt{5})/2$. Each of 20 faces of the icosahedron is then tessellated with a triangular grid with $10(n-1)(n-2)$ interior sites, where n is the number of times the grid cuts the side of a triangular face. For $n = 65$, the total number of sites of the mesh is $N = 12 + 30(n-1) + 10(n-1)(n-2) = 42252$. The grid points are then spherically projected into the sphere centered at (0,0,0). For nearest-neighbor interactions all sites are sixfold coordinated, except for the 12 original vertices of the icosahedron, which have five nearest neighbors. (This produces a lattice whose bonds are in an interval between 1.388×10^{-2} and 2.037×10^{-2} rad for $n = 65$.) The Gaussian curvature of a sphere with radius R is given by $K = R^{-2}$. We investigated grain growth on a surface of a unit sphere, $K = 1$, for two values of stiffness constant, $c = 0.002$ and 0.0002. This approach is equivalent to studying grain growth on spheres with the same properties but with different sizes, where smaller value of c corresponds to larger value of R.

Figure 1 shows the time dependence of the mean grain size $A_{\rm av}$ for five different runs for the two values of c. Clearly, a non-power-law growth behavior is observed. Following some initial curvature, all curves reach a local maximum, then decline, and finally rise steeply to reach its maximum attainable value N. The final state of microstructure consists of just one "singular" grain. Using the same sequence of random numbers it is possible to repeat a run and to monitor the time evolution of the domain that ultimately engulfed entire surface.

In Figs. 2(a) and 2(b) we present results for mean grain size $\langle A_{\rm av} \rangle$ the grain size of the singular grain $\langle A_1 \rangle$ and rate of change of "singular" grain size $\langle dA_1/dt \rangle$ for microstructures corresponding to the two spherical surfaces and averaged over five runs. (The discontinuous "steps" seen in the plots of A_1 vs t are due to the accounting procedure described at the end of Sec. II.) Clearly, in the early stages of coarsening the absolute difference between $\langle A_1 \rangle$ and $\langle A_{\rm av} \rangle$ is less than one order of magnitude, although it does slowly increase with t. In the same regime the rate of increase in $\langle A_1 \rangle$ is approximately constant. At a critical value of t^*, when $\langle A_{\rm av} \rangle$ reaches a local maximum, the singular grain rapidly increases in size so

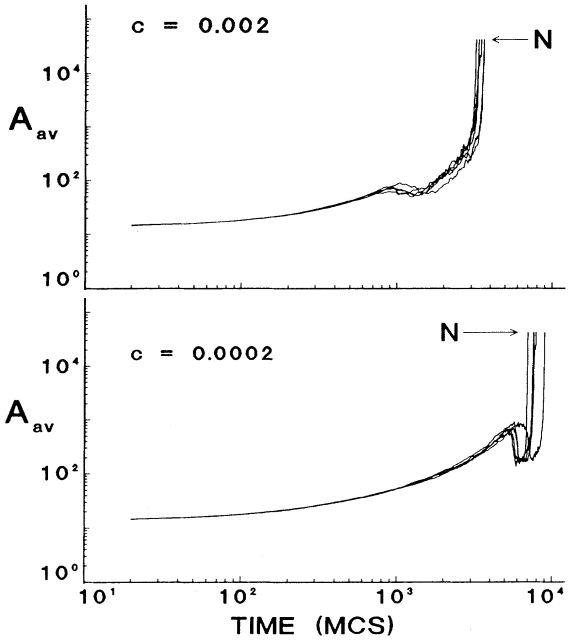

FIG. 1. Log-log plot of mean grain size A_{av} vs time for a spherical surface with stiffness constant $c=0.002$ and 0.0002 obtained for five different Monte Carlo runs. The maximal value of A_{av}, $N=42\,252$, is denoted by arrows.

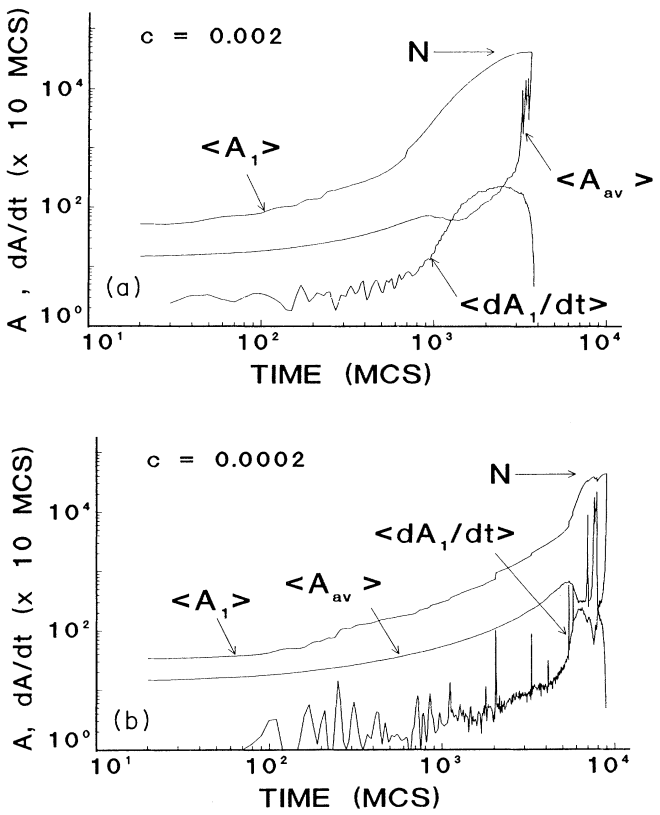

FIG. 2. Logarithmic plot of mean grain size $\langle A_{av} \rangle$, "singular" grain size $\langle A_1 \rangle$, and speed of increase of abnormal grain size $\langle dA_1/dt \rangle$ vs time, averaged cover five runs, for a spherical surface with stiffness constant (a) $c=0.002$ and (b) $c=0.0002$.

that $\langle dA_1/dt \rangle$ changes by almost two orders of magnitude. Only at very late stages of coarsening when singular grains cover most of the surface does the rate of expansion decrease to the initial level. The qualitative change in coarsening that occurs at t^* occurred when the value of the Gaussian curvature field of grain 1 of size $A_1(t^*)$ is larger than the corresponding value of the surrounding matrix grains of size $A_{av}(t^*)$ by about $E^*=2J$ per site. This can be understood by noting that mesh of sites representing the spherical surface is almost everywhere equivalent to a triangular lattice. It has been demonstrated elsewhere [45], that for the triangular lattice with nearest-neighbor interaction a grain with "stored" energy advantage of $E^*=2J$ per site will grow homogeneously into the surrounding matrix. The condition can be expressed as $c\Delta A(t^*)\cong 2$, where $\Delta A(t^*)=A_1(t^*)-A_{av}(t^*)$ or, since $A_1(t^*)\gg A_{av}(t^*)$, as $A_1(t^*)\cong 2/c$. For $c=0.002$ and $c=0.0002$, corresponding values of t^*, 720 and 5760 MCS, are indeed consistent with local maxima of $\langle A_{av} \rangle$. It is worth noting that the decease in $\langle A_{av} \rangle$ for $t \geq t^*$ is due to an increase in number of few-sided grains that are created during rapid advancement of singular grain boundary into the matrix. This results in fluctuations of the grain-boundary profile which have the same time scale for both transverse and longitudinal directions and occasionally lead to creation of few-sided grains in vicinity of the grain boundary. Naturally, this effect does not occur in soap froths, where the characteristic time of longitudinal fluctuations, or "warping," is much smaller than the time scale of transverse fluctuations, which is related to fluctuations in gas pressure in bubbles. However, this effect does not significantly change the long-time behavior of grain ensembles and can be safely ignored in the present study.

The above observations are confirmed by studying the grain-size distributions for corresponding microstructures. Figures 3(a)–(3f) show double-logarithmic diagrams of relative frequency of grains as a function of their relative size $\langle A \rangle / \langle A_{av} \rangle$ for $c=0.002$. Clearly the initial distribution of grain sizes, Fig. 3(a), can be well approximated by a parabola, i.e., it can be represented by a normal distribution with a second moment μ less than 1, on a semilogarithmic plot [2,3]. Deviations from this distribution are visible at small values of grain size and have its origin in the above described thermal fluctuations. At later times $0<t<t^*$, Figs. 3(b)–3(c), the second moment slightly increases, but the distribution preserves its normal character. At these times the singular grain remains comparable in size with other large grains that are typically 10 times larger than A_{av}. Only when the singular grain reaches the critical size necessary for its homogeneous expansion does the distribution change qualitatively in character, Figs. 3(d)–3(e). It then becomes multimodal, i.e., it contains numerous small grains and very few grains with a much larger than average grain size. Also, the relative number of grains of intermediate size decreases with time, Fig. 3(f).

Additional insight into the nature of grain coarsening

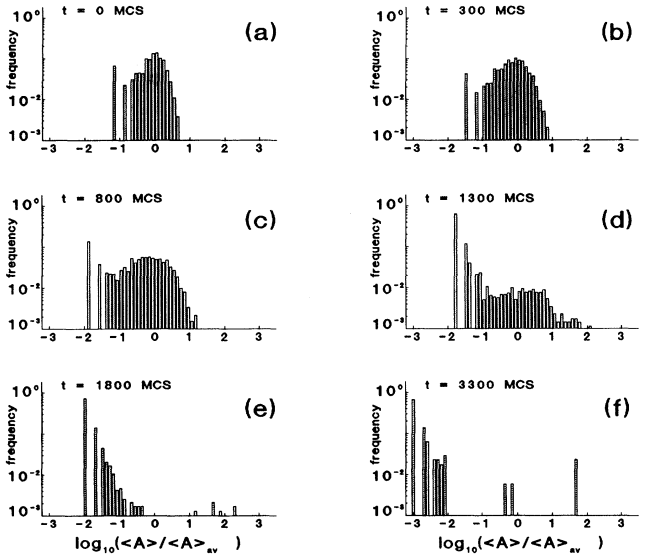

FIG. 3. Logarithmic plot of distribution of grain sizes at surface with $c=0.002$ measured at $t=0$, 300, 800, 1300, 1800, and 3300 MCS and averaged over five runs.

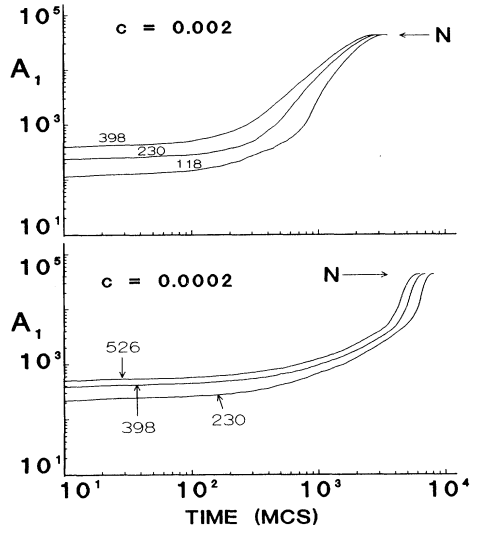

FIG. 4. Log-log plot of a cap size A_1 vs time for a spherical surface with $c=0.002$ and 0.0002 obtained for three runs with caps of initial sizes of 118, 230, 398 and 230, 398, 526, respectively.

on a spherical surface may be gained by studying the behavior of a microstructure consisting of one, large grain with $S=1$ and introduced into a matrix built of much smaller grains with orientations of $S=2,3,\ldots,48$. Figure 4 shows the results for individual runs when a single-grain "cap" with sizes between $188\cong 2.79\times 10^{-3}N$ and $526\cong 1.24\times 10^{-2}N$ were placed in a matrix of grains with $A_{\rm av}(t=0)=14\pm 10$. Plots of A_1 vs t have a characteristic sigmodial shape, quite similar to those shown in Fig. 2. Also, the time evolution of "caps" with large initial sizes are markedly flattened. Interestingly, the value of the time difference $\Delta t=t_f-t^*$, where t_f is the total time of coarsening, is almost independent of the "cap's" size. For $A_{\rm cap}=150$, 230, and 398, Δt is 2880(50), 2880(50), and 2850(20) MCS, respectively. (The figures in parentheses indicate the level of error associated with the quoted values.) Calculating the same quantity for $c=0.002$ yields for $A_{\rm cap}=280$, 398, and 526, Δt of 2980(80), 2850(80), and 2780(70) MCS, respectively. Also, the result suggests that while Δt is only weakly dependent on c, the time evolution of a "cap" grain is sensitive to the stiffness constant. Figure 5 shows qualitatively different behavior of cap grains with $A_{\rm cap}=230=5.44\times 10^{-3}N$, obtained in five different simulations for $c=0.002$ and 0.0002. It is seen that on a sphere with $c=0.0002$, in all five runs, caps became singular grains engulfing the entire surface. Similar runs carried out on a sphere with $c=0.0002$ resulted in only one case when the cap engulfed the surface. In all other runs, the cap grew in a similar fashion but finally collapsed, apparently consumed by another singular grain. This difference can be explained by noting that a small value of stiffness constant c leads to coarsening in which a cap reaches an advantage over the matrix grains, in terms of Gaussian curvature energy, at relatively late times $t^*=pt_f$, $p\cong 1$. Until then, coarsening occurs *via* quasi-normal growth, which leads to a fast growth of small grains and a comparatively slow increase in the size of large grains. As a result, at time t^*, the microstructure consists of more than one grain of a "subcritical" size, $A\cong A^*$, each of which may finally become a singular grain. This scenario agrees with the results of simulations of abnormal grain growth in a two-dimensional matrix where the driving force is provided solely by curvature [46]. Srolovitz, Grest, and Anderson found that in this case the normal grain-size distribution is very robust and resistant to perturbations. In particular, the power-law growth for a cap grain which is much larger than all its neighbors, is never observed. The results show that

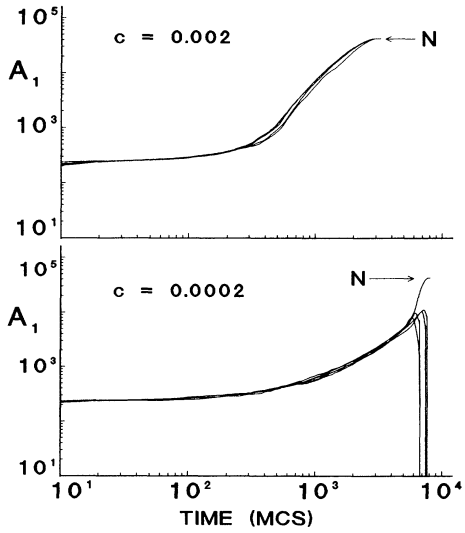

FIG. 5. Log-log plot of a cap size A_1 versus time for a spherical surface with $c=0.002$ and 0.0002 obtained for five runs with the same initial size of the cap, $A_1(0)=230$.

the time-averaged growth rate is significantly lower than the mean growth rate for the remaining microstructure and that it decreases as the initial A_1 is made larger. The difference in size between cap grain and the mean grain size deceases with time until it is absorbed into the normal grain-size distribution. These observations correspond to results found in the present model in the limit $c \to 0$.

The above reasoning implies that, for each value of the stiffness constant, there exists a critical size $A^* = A^*(c)$ such that a cap with $A > A^*$ will always become a singular grain. Moreover, $A^* = A^*(c)$ is expected to be a decreasing function of c. In order to investigate this relation, runs were carried out with different size caps. For $c = 0.002$, in all five runs the cap was able to become a singular grain if its size was 230 or larger, although in some cases caps as small as 118 could engulf the whole surface. For $c = 0.0002$, the cap had to be at least 526 $= 1.24 \times 10^{-2} N$ to consume the surface although, occasionally, caps with $A_{\text{cap}} = 230$ managed to engulf the surface. Indeed, the critical value of an "abnormal" grain A^* is a decreasing function of the stiffness constant. A more precise determination of the dependence was difficult due to relatively large statistical scatter in measurements of A^*. An approximate form of this dependence may be obtained in a manner similar to that carried out for an "abnormal" grain and leads to the expression $A^* \equiv A(t^*) \cong 2c^{-1}$.

Clearly, the observed behavior of the grain ensemble on the surface with positive Gaussian curvature resembles abnormal (or secondary) growth which is observed in polycrystals upon annealing and has been extensively studied in the past [46–49]. It was originally thought that grains with particular crystallographic orientations may have lower surface energies or higher mobilities and, hence, are able to acquire a size advantage over all other grains. Moreover, a grain having a large initial size advantage was not observed to be a sufficient condition for abnormal grain growth [46,49]. This is because the modifications introduced in these models had local character. The present model recognizes that Gaussian curvature is a global quantity and, hence, must be modeled differently, resulting in qualitatively different kinetics. In contrast to local abnormal grain-growth models, a grain with a sufficient size advantage will grow exponentially fast into the matrix. On a curve surface, as shown here, one does not need to favor any particular orientation to result in an ensemble of grains which become unstable against small perturbations, making it qualitatively different from previous, local models.

IV. RESULTS FOR THE TOROIDAL SURFACE

In this study a 200×200 triangular lattice with a periodic boundary condition was used to represent the surface of a torus. A torus was chosen since it is the simplest surface with a varying Gaussian curvature. The saddlelike shape of the "interior" of a torus is characterized by its negative curvature, while the curvature of the exterior is positive, Fig. 6(a). It is worth noting that although a triangular lattice with a periodic boundary condition is topologically equivalent to a toroidal surface, the corresponding Potts model, Eq. (3), describes domain growth very well on a flat surface, suggesting that lattice connectivity alone does not ensure the correct dynamic behavior on a curved surface. The Gaussian curvature of a torus's surface can be found in terms of the coefficients of the first and second Gauss differential forms [50]. In

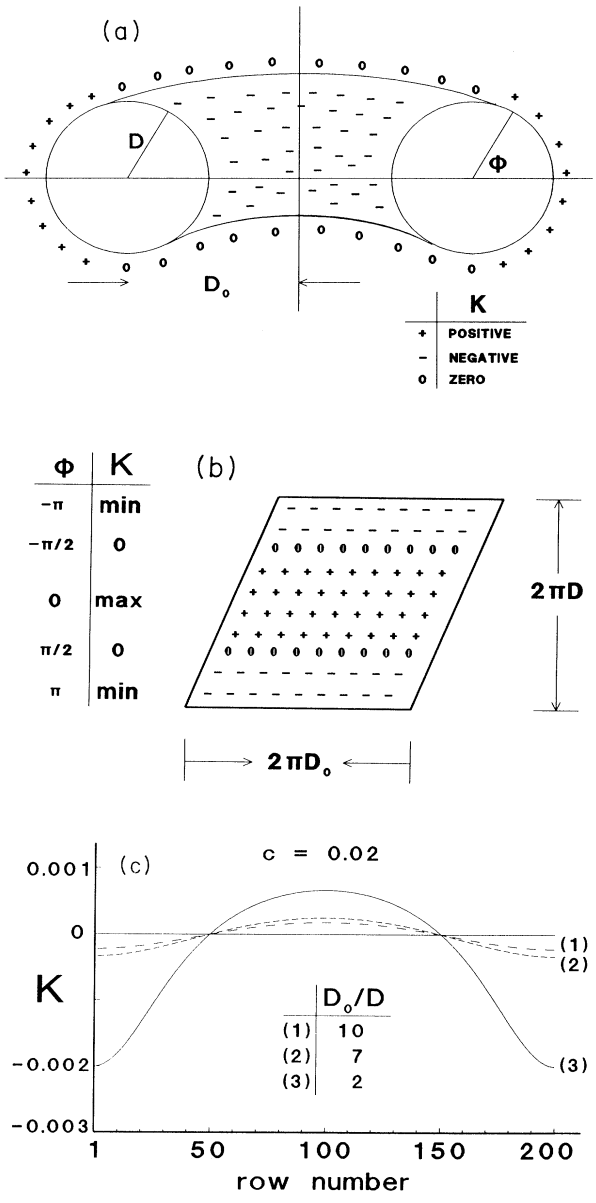

FIG. 6. (a) A schematic representation of a torus with principal radii D_0 and D. The $+$, 0, and $-$ symbols depict regions of toroidal surface with positive, zero, and negative values of Gaussian curvature, respectively. (b) A schematic representation of the torus via a triangular lattice. The table on the left shows schematically values of angle ϕ and Gaussian curvature K corresponding to different lattice rows. (c) Gaussian curvature K vs row number for $c = 0.02$ and three values of principal radii ratio $D_0/D = 2$, 7, and 10.

the case when the equation of a surface is given explicitly by $z=f(x,y)$, the Gaussian curvature K is given by

$$K=\frac{U_{xx}U_{yy}-U_{xy}^2}{V_{xx}V_{yy}-V_{xy}^2}\ , \tag{7a}$$

where

$$\begin{aligned} U_{\alpha\beta}&=f_{\alpha\beta}(1+f_x^2+f_y^2)^{-1/2}\ , \\ V_{\alpha\beta}&=\delta_{\alpha\beta}+f_\alpha f_\beta\ , \\ f_\alpha&\equiv\frac{df}{d\alpha},\quad f_{\alpha\beta}\equiv\frac{d^2f}{d\alpha\,d\beta}\quad(\alpha,\beta=x,y)\ , \end{aligned} \tag{7b}$$

and $\delta_{\alpha\beta}$ is the Kronecker delta. If the equation of the torus is given as $D^2=z^2+[D_0-(x^2+y^2)^{1/2}]^2$, where D, D_0 are, respectively, the internal and external radii of a torus, see Fig. 6(a), then Eqs. (7a) and (7b) lead to the Gaussian curvature at a point on the surface

$$K=\frac{1}{D^2}\frac{\cos\phi}{\frac{D_0}{D}+\cos\phi}\ , \tag{8}$$

where ϕ is the angle between the vector $t\equiv[x,y,0]$ lying in the plane OXY and a normal vector to the surface of the torus at a point with the Cartesian coordinates (x,y,z). From this formula it is easy to see that the Gaussian curvature retains the cylindrical symmetry of a surface, and is positive on the outside of the torus, $-(\pi/2)<\phi<(\pi/2)$, and negative on the inside of a torus, $(\pi/2)<\phi<(3\pi/2)$, see Fig. 6(b). Moreover, integrating over the entire torus surface, the Gaussian curvature vanishes. We investigated grain growth on a toroidal surface with stiffness constants $c=0.02$ and $D=1$ for three values of $D_0/D=2$, 7, and 10. In Fig. 6(c) we present plots of K for row numbers 1–200 where row no. 1 corresponds to a line of largest negative curvature, i.e., the inner equator at the torus. It is important to note that representing the toroidal surface by an $L\times L$ triangular lattice introduces distortions so that the sites in a saddlelike region have smaller Voronoi cells (i.e., one-site grains on a dual lattice) than sites in the region with maximal values of K. In principle, this effect should be included in the model by assigning each lattice site a value of Gaussian curvature energy weighted by relative size of its Voronoi cell so that the sum of all curvature energies over N lattice sites would correctly yield zero. In order to simplify our calculations we did not consider these correction factors, which are seen, in Fig. 6(c), to be small for tori with $D_0/D\geq 7$.

Figures 7(a) and 7(b) and 8(a) and 8(b) show snapshots of microstructures, presented here as flat meshes, corresponding to tori with $D_0/D=2$ and 10, respectively. Both initial configurations, Fig. 7(a), are uniform. However, very soon one begins to see qualitatively different behavior in the two regions. The central section, corresponding to $K>0$, coarsened much faster than the lower and upper regions characterized by $K<0$. The inhomogeneity advances much faster on the strongly curved toroidal surface with $D_0/D=2$ than for $D_0/D=10$, Figs. 7(a) and 8(a). In both cases, the outside of the torus, represented by lattice rows between 50 and 150, rapidly evolved toward a few-grain configuration and ultimately to just a single grain, Figs. 7(b) and 8(b). It is worth noting that at the intermediate coarsening stage, boundaries of a few large grains occupying regions with $K>0$ became rough and are decorated with many few-sided grains, e.g., configurations at $t=3800$ and 5800 MCS in Fig. 7(b) and at $t=13\,800$ MCS in Fig. 8(b). This event is reminiscence of coarsening at spherical surfaces at times $t>t^*$, consistent with the fact that in both cases coarsening occurs in positively curved regions of the surface. Evolution of grains in the saddlelike regions of the lattice with negative curvature, led to stable-size grains which, in the asymptotic regime, are equiaxed with almost-hexagonal shapes. For $D_0/D=10$, grains in this region reach a relatively large size. They are also larger in regions near $K\cong 0$ then in regions characterized by large values of $|K|$. This is clearly visible for a mesh with $D_0/D=10$.

The above observations can be made more quantitative

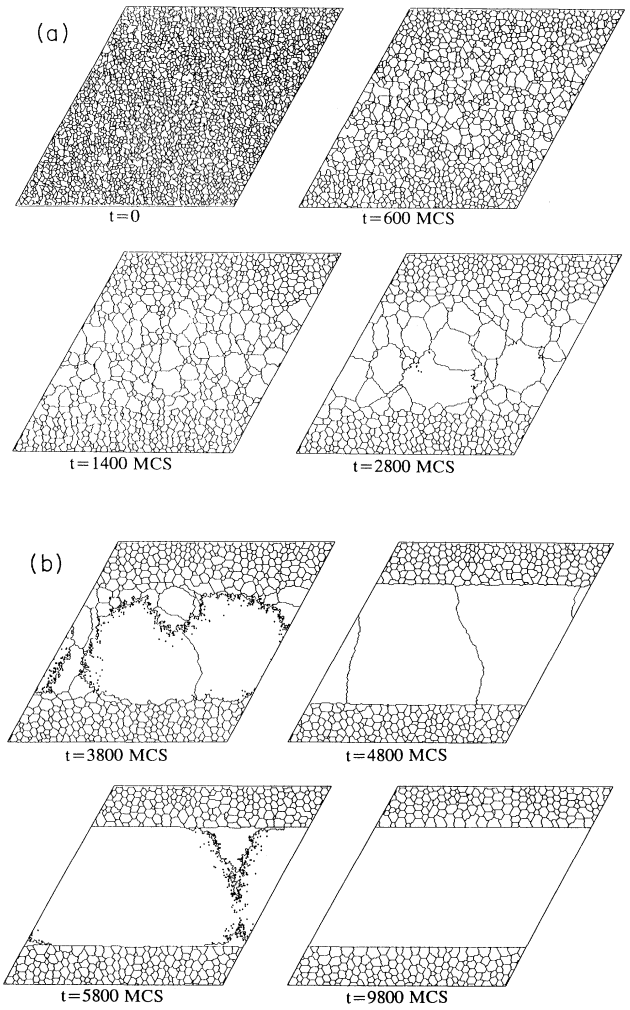

FIG. 7. The time evolution of a microstructure on a toroidal surface with $D_0/D=2$ and stiffness constant $c=0.02$ measured at $t=0$, 600, 1400, 2800, 3800, 4800, 5800, and 9800 MCS.

by considering the time evolution of A_r, the mean size of a grain occupying lattice region in vicintiy of rth row, defined as $A_r=(1/L)\sum_{i=1}^{L}A_r(i)$ wher $A_r(i)$ is size of a grain with one of its sites at column i and row r. Here, $L=200$. In Figs. 9(a) and 9(b) we display semilog plots of time dependence of $\langle A_r \rangle$ averaged over five different runs, for several Monte Carlo time steps. It is seen that the fast growth of grains at the outside of a torus is uniform throughout the region of positive curvature. It is important to observe that the "abnormal" grain covers not only the whole outside of torus but also the two adjacent regions with $K<0$, but small in magnitude. The reason for this intrusion can be understood by considering what happens when site i of grain α of N_α sites, in the vicinity of the $K=0$ boundary, is next to an abnormally large grain β of N_β sites ($N_\alpha \ll N_\beta$). If site i attempts to change its orientation to that of grain β, simple analysis shows that the energy cost $-\delta H$ to reorientation of S_i is $-\delta H \approx -c(\kappa_\beta + K_i N_\beta)$. Since κ_β, the energy field of βth grain, can be much larger than the energy term of αth grain and the abnormal grains may grow into regions of $K<0$, the flip will be facilitated at sites with $K_i<0$ if

$$|K_i| \le \frac{\kappa_\beta}{N_\beta} \approx \bar{\kappa} , \tag{9}$$

where $\bar{\kappa}=(1/f_a)\sum_i K_i$ is the average value of Gaussian curvature energy in an abnormally large grain which occupies the $f_a \equiv (N_\alpha/N) \ge 0.5$ fraction of all lattice sites. The quantity f_a is an increasing function of D_0/D as can be seen by solving a continuous form of Eq. (9) which is equivalent to the inequality $|\phi| \le \phi_a$ where ϕ_a is given by

$$-\frac{\cos\phi_a}{D_0+\cos\phi_a}=2\phi_a-\frac{4D_0}{\sqrt{D_0^2-1}}\left\{\tan^{-1}\left[\left[\frac{D_0-1}{D_0+1}\right]^{1/2}\tan\frac{\phi_a}{2}\right]\right\} . \tag{10}$$

Here, we have taken $D=1$. It is easy to see that $\phi_a(D_0)$ is an increasing function of D_0 and that for $D_0 \gg 1$, Eq. (10) reduces to $-\phi_a=\tan\phi_a$ where a solution is $\phi_a=2.02875\ldots$. Since $\phi_a=\pi[(2r_a/L)-1]=\pi f_a$, where r_a is corresponding lattice row number the max-

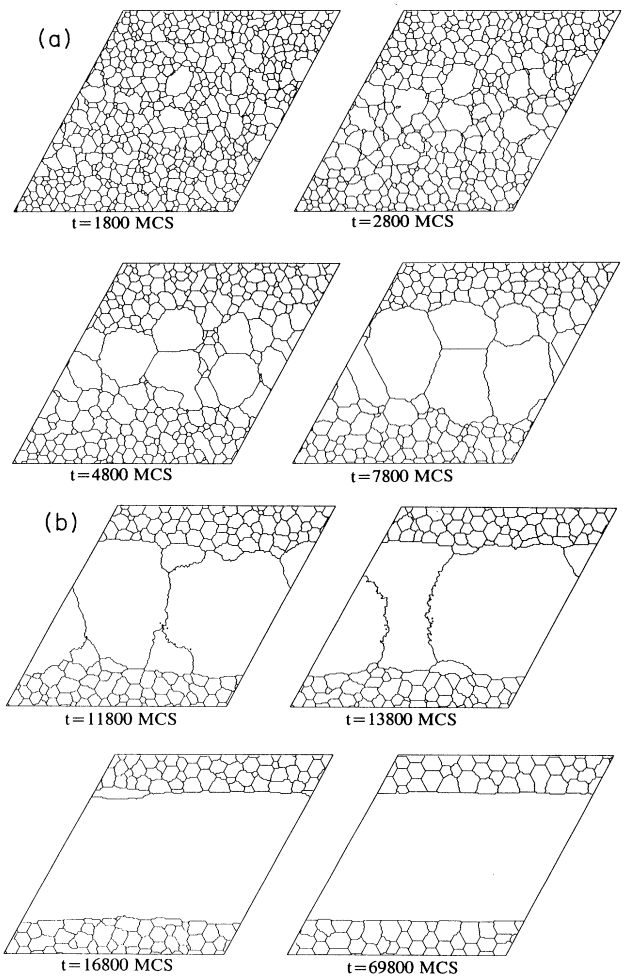

FIG. 8. The time evolution of a microstructure on a toroidal surface with $D_0/D=10$ and stiffness constant $c=0.02$ measured at $t=1800$, 2800, 4800, 7800, 11 800, 13 800, 16 800, and 69 800 MCS. The initial configuration, at $t=0$, is the same as in Fig. 7.

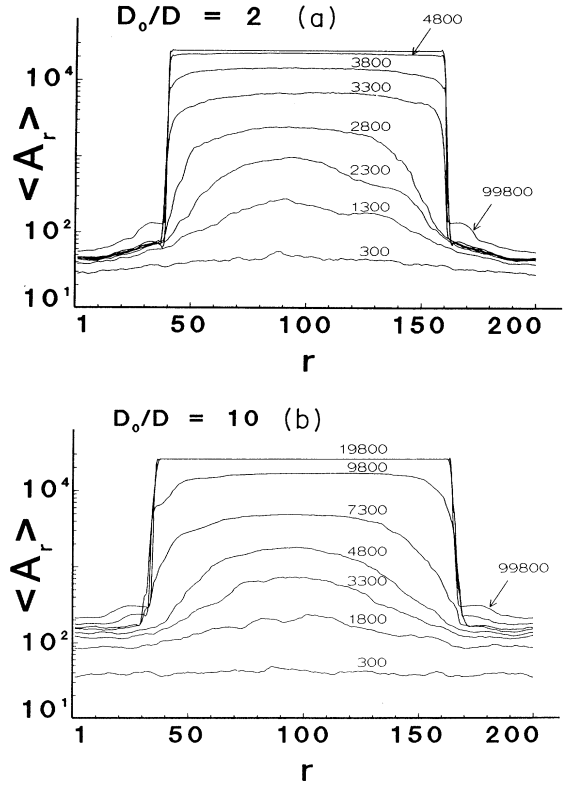

FIG. 9 Semilogarithmic plot of $\langle A_1 \rangle$, mean size of a grain localized in the vicinity of an rth row of a lattice representing surface of torus with $c=0.02$ and the principal radii ratio (a) $D_0/D=2$ and (b) $D_0/D=10$, obtained for times between 300 and 99 800 MCS, averaged over five Monte Carlo runs.

imum value of $\phi_a(D_0)$ is $\phi_a=0.64577\ldots$. Moreover, for $D_0=2$, 7, 10 the value of $\phi_a(D_0)$ found from Eq. (10) is 0.5980, 0.6279, and 0.6328, respectively. These values are only slightly smaller than the corresponding values found in our simulations: $\phi_a(2)=0.6050(1)$, $\phi_a(7)=0.6381(7)$, $\phi_a(10)=0.6460(6)$. The small differences between these values is most probably due to approximations made in derivation of Eq. (9) and to the finite value of T which facilitates site reorientations to energetically unfavorable orientations. The most interesting result of the above analysis is the observaton that on *any* toruslike surface the abnormally large grain will have a relative size larger than the expected value of 0.5. In particular, on the surface of only slightly bent cylinder, where $D_0/D \gg 1$, a characteristic bimodal distribution of grain sizes will develop with abnormal grain covering $\phi_a=0.64577$ of the entire surface. However, testing this prediction may be difficult since for a given microstructure the critical grain size A^* depends on the constant c. If c is very small, the surface may be too small to exhibit the expected behavior and only quasinormal grain growth will be observed.

The above conclusion may explain difficulties in obtaining reproducible results encountered by researchers investigating grain growth in thin polycrystalline layers on curves substrates. Recently Levin, Avron, and Brokman [29] reported preliminary experimental observations on grain morphology in acoiled supported thick layers of Pb–0.2 wt % Sb. Metallurgical inspection revealed the presence of a bimodal grain size pattern, similar to that found here at the toroidal surface but the researchers were unable to reproduce the observations in other systems. It is conceivable that the unique result was not due to the Gaussian curvature but other mechanisms, e.g. drag effects due to impurities [29]. It is possible, however, that small value of the Gaussian curvature contributed to reported difficulties.

Figures 9(a) and 9(b) show also that stable microstructure that is found inside of torus after simulation is characterized by a mean grain size $\langle A_r \rangle$ that is, as expected, an increasing function of D_0 and an increasing function of parameter $|\phi|$. However, the evolution of grains in negatively curved regions of the torus is relatively slow and even after 10^5 MCS there is an evidence of

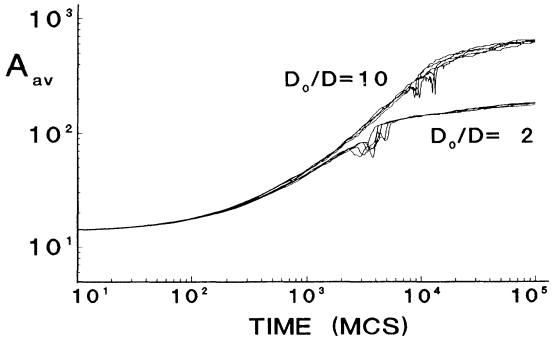

FIG. 10. Logarithmic plot of mean grain size A_{av} vs time obtained for five runs for a torus with the principal radii ratio $D_0/D=2$ and 10.

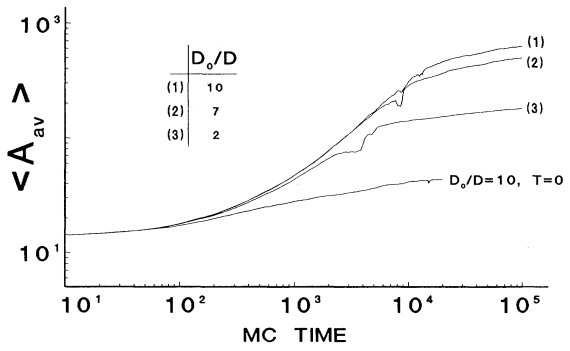

FIG. 11. Logarithmic plot of mean grain size $\langle A_{av} \rangle$ vs time obtained from five runs at $T=0.231T_c^{\Delta}$ and surfaces with the principal radii ratio $D_0/D=2$, 7, and 10. Also shown is a similar plot obtained from five runs at $T=0$ and $D_0/D=10$.

a slight increase in grain size. This can be better seen from Fig. 10 which present time evolution of average grain size for $D_0/D=2$ and 10, respectively, for five Monte Carlo runs. A slight dip in these curves at times between 3×10^3 and 2×10^5 MCS correspond to a rapid increase in the number of few-sided grains that occured at $t\cong t^*$. In Figure 11 we present the time evolution of $\langle A_{av} \rangle$ averaged over all configurations. Also shown is the behavior of $\langle A_{av} \rangle$ for $D_0/D=10$ where site reorientation to energetically unfavorable configurations is suppressed, i.e., for $T\cong0$. It is found in this case that bimodal grain-size distribution consists of the ensemble of very small grains, with sizes typically one order of magnitude smaller than comparable sizes of grains obtained in simulations for $T>0$. This is clearly due to the lack of thermal fluctuation which can overcome local energy minima of metastable states.

V. SIMULATIONS ON A PSEUDOSPHERE

Another approach to the simulation of dynamical effects due to Gaussian curvature is to study the standard Potts model on an isotropic lattice of appropriate symmetry. For a surface of constant curvature this can be achieved by finding its regular tessellation. A regular tessellation is a covering of the entire plane by nonoverlapping, regular polygons meeting only along complete edges, or at vertices [39]. All polygons in any one tessellation must have the same number of edges. It is easy to show that a regular tessellation of the plane with q regular p-sided polygons (p-gons) meeting at each vertex (and denoted by $\{p,q,\}$) has the property [39]

$$(p-2)(1-2)\geq 4\ , \tag{11}$$

where the inequalty and equality signs correspond to the Euclidean ($\mathbb{R}^2$) and hyperbolic planes, respectively. It follows, there are just three regular tessellations of the $\mathbb{R}^2$ plane, namely $\{4,4\}$, $\{6,3\}$, and $\{3,6\}$. However, there is an infinite number of possible regular tessellations of the hyperbolic plane. The hyperbolic plane is a surface embedded in a space with a Minkowski (hyperbolic) metric. (In contrast to the surface of a positive Gaussian curvature, which can be embedded in a three-dimensional Eu-

clidean space, a global embedding is prohibited for surfaces of negative curvature [51].) It follows, that for a surface of a constant, negative Gaussian curvature (pseudosphere) there is an infinite number of regular tessellations which can be used to formulate an appropriate Potts-model Hamiltonian.

In this study, we constructed an octagonal $\{8,8\}$ tessellation of a pseudosphere, which in the following will be represented by the Poincaré disk model [52]. The starting point of the construction was to select the regular octagon, having vertex angles $2\pi/8$ and area 4π, as a fundamental domain. The group of isometries (displacements) of the pseudosphere is the ortochronous Lorenz group and its discrete subgroup G can be used to create identical replicas of a fundamental domain which tessellate the pseudosphere. The fundamental displacements are produced by the four special boosts g_0, g_1, g_2, g_3, and their inverses that exchange opposite sides of a fundamental domain [52]. Explicitly,

$$g_j=\begin{bmatrix} 1+\sqrt{2} & e^{(ij\pi/4)}\sqrt{2+\sqrt{2}} \\ e^{-(ij\pi/4)}\sqrt{2+\sqrt{2}} & 1+\sqrt{2} \end{bmatrix}, \quad j=0,1,2,3 \tag{12}$$

where $i\equiv\sqrt{-1}$. An element G^r of non-Abelian subgroup G is obtained by successive application of the g_j and g_j^{-1}, i.e., $G^r=\prod_{\alpha=i_1}^{i_r} g_\alpha$, $g_\alpha=g_0,g_0^{-1},g_1,g_1^{-1},\ldots$. In order to generate a list of vertices used to build the lattice we implemented an alternative procedure where all elements $\{G^r:r=0,1,\ldots,6\}$ of the subgroup G were applied to a fundamental vertex $O(0,0)$. This method utilizes the fact that the octagonal lattice is self-dual. The procedure gave a lattice with $N_6=155\,577$ points most of which, however, were boundary sites with just one nearest-neighbor (NN) site, see Fig. 12. Only 22 289 of all sites had 8 neighbors, whereas 336 were twofold coordinted. Unfortunately, we were unable to find an easy way to implement the periodic boundary condition and to close the lattice on itself. In order to alleviate the influence of the boundary sites we pruned the lattice of all "dangling" bonds. This procedure left less than 2% (2289) of N_6 sites, which formed a noncompact network of 392 connected octagons. Only the eight central octagons adjacent to $O(0,0)$ had all eight nearest-neighbor octagons. The remaining octagons formed a fractallike pattern decorating the central rosette. This can be checked by analyzing the connectivity of octagonal network that included 65 sites with 8 NN, 392 sites with 3 NN, and 1832 sites with 2 NN. The lattice construction was carried out using a simple distance checking algorithm and took about 40 h of CPU on a HP 9000/750 workstation. Since the time needed to create the lattice using the subgroup $\{G^r\}$ grows like 7^{2r}, we did not attempt to create a lattice corresponding to $r=7$ or larger.

The kinetics of the grain-boundary motion was simulated by the finite-temperature Metropolis Monte Carlo method with the Glauber excitation mechanism, described in Sec. II. Simulations started from a completely disordered state and were quenched to $T\cong 0$, $0.145J$, $0.193J$, and $0.217J$, which is about 0, $0.3T_c^\infty$, $0.4T_c^\infty$, $0.45T_c^\infty$, and $0.60T_c^\infty$ respectively. (T_c^∞ is the critical temperture for an infinite lattice [53].) Figure 13 shows the time dependence of the mean grain size averaged over five different runs on an octagonal lattice with 2289 sites. Here, a distinctively non-power-law growth behavior is observed. Following some initial curvature all curves reach, at $T\cong 2500$ MCS its maximum $A_{\max}(T)$ which is a decreasing function of temperature. For all temperatures, however, $A_{\max}<57$, the number of sites in an eight-octagonal rosette. Similar simulations carried out with use of a lattice with all 155 557 sites yielded microstructures with almost all sites forming one and two-site domains. This effet is ascribed to the influence of lattice boundary sites.

The observed saturation of grain size cannot be attributed solely to the influence of the Gaussian curvature of the tiled surface or to the edge effets. It turns out that the grain growth on an octagonal lattice is inherently prone to pinning due to topology of the lattice itself. This can be explained by investigating the behavior of triple vertices on the lattice at $T=0$. It is known [54] that on a triangular lattice with NN interaction, in the absence of thermal fluctuations, pinning does not occur despite the fact that vertices V_{222}, where three grains meet at angles of 120°, cannot move, Fig. 14(a). It implies that the population of vertices on a triangular lattice can-

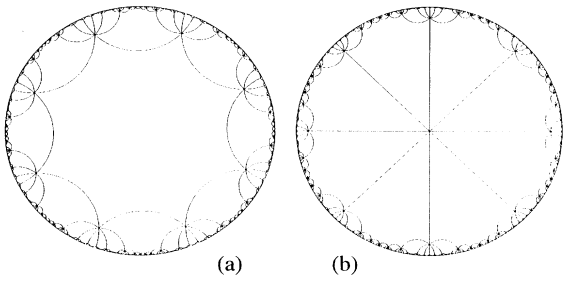

FIG. 12. The octagonal network obtained on the pseudosphere by successive application of fundamental boosts g_0, g_1, g_2, g_3 and their inverses to (a) a fundamental domain and (b) a fundamental vertex (see the text). A tessellation is shown in the Poincaré disc (compare Ref. [52]).

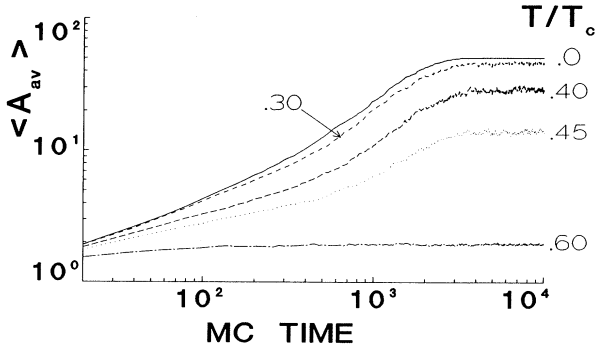

FIG. 13. Log-log plot of mean grain size $\langle A_{\rm av}\rangle$ vs time obtained from five runs at $T=0$, $0.3T_c^\infty$, $0.4\ T_c^\infty$, $0.45T_c^\infty$, and $0.6T_c^\infty$ and the octagonal lattice with 2289 sites.

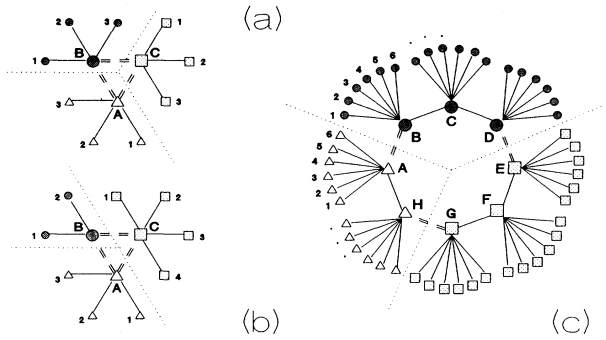

FIG. 14. A schematic representation of triple vertices on the triangular, (a) and (b), and octagonal (c) lattice. The dotted line delineates grain boundaries, the letters $A-H$ denote sites of an elementary plaquette dual to a vertex, and the numbers correspond to their remaining NN. (a) Each spin on one of three sites representing a V_{222} vertex is pinned by three like spins on NN sites. (b) Vertices V_{123} or V_{321} are able to move since the energy cost of flipping a spin at site B is zero. (c) None of the spins at sites A, H, G, E, D, B can flip due to presence of like spins at seven of their NN sites.

not include only V_{222} vertices. This observation is directly related to the fact that hexagonal grains of *different* sizes cannot tile a flat surface [40,55]. (For this to be true, a necessary condition is that the equal-size grains that meet at a vertex must fit into a larger grain of the same shape.) It follows that a microstructure on a triangular lattice must also include other triple vertices: V_{123} and V_{321}, where three grains meet at angles of 60°, 120°, and 180°. These vertices, however, are mobile [Fig. 14(b)] and promote coarsening. Similar analysis carried out for the octagonal lattice is more difficult due to a larger number of possible nontrivial triple vertices. Clearly, the energy minimizing grain shape on the lattice is an octagon. This results in coarsened microstructures similar to that shown in Fig. 14(c), with grains having most of their vertex sites connectd to six interior sites. It contrast to a triangular lattice, *all* these vertices, $V_{ijk}(i+j+k=8,\ ijk>0)$, are pinned in the absence of thermal fluctuations. (We also observe in passing that on the octagonal lattice there is no pinning of ledges.) It follows that in order to avoid the pinning and to be able to investigate the dynamical effects on the octagonal lattice due solely to the Gaussian curvature it is necessary to include the next-nearest neighbors (NNN) or, possibly, even further range of interactions in the Potts-model Hamiltonian. Due to a small size and noncompact shape of the lattice availabe to us, we did not pursue the study in this direction.

It is worth noting that octagonal domains of different sizes cannot tile the pseudosphere. A justification of this conjecture can be made by considering a rosette built of eight octagons of equal size meeting at a vertex $O(0,0)$, Fig. 12. Let OV be a common edge of two adjacent octagons, $OVA_1A_2A_3A_4A_5A_6$ and $OVB_1B_2B_3B_4B_5B_6$. The angle between edges VA_6 and VB_6 is $2\times 2\pi/8$, which is larger than $2\pi/8$ but smaller than π. As a result, the rosette cannot be covered by a larger octagon, which points to correctness of the conjecture. This result is important, since it implies a lack of a one-to-one correspondence between the pinning of grain growth and existence of a frozen state consisting of all domains in local equilibrium. This hypothesis, postulated recently [56,57] for two-dimensional domain growth simulated by the Monte Carlo, method apparently holds only for grains covering flat surfaces. The local equilibrium shapes, here octagons, cannot tile the hyperbolic surface. Although the thermodynamic force of curvture can propagate kinks along the domain walls, it cannot move them through vertices between adjacent domains. This leaves all the domains in the state of metastable equilibrium, i.e., curvature-driven growth becomes frustrated.

The zero-temperature equilibrium shapes change at sufficiently high temperatures approaching the shape that minimizes the perimeter length, i.e., a circle [36]. It is easy to see that the energy cost of flipping one corner of an octagonally shaped domain, immersed in a sea of spins with other orientation, is $4J$. Once the corner spin flips, a kink is created which can propagate freely along the edge, i.e., edges can flip without the energy cost. Thus, shrinking the octagon involves crossing a number of energy barriers of $E=4J$. This implies that such corner flips should occur regularly on time scales much longer than $\tau=\exp(4J/T)$ (Refs. [56,57].) For $T\cong 0.9T_c^{\infty}\cong 0.43J$, τ is about 10^4 MCS, so that runs at least 10^5 MCS were needed to observe domain coarsening. (Here it was assumed that the described process is a necessary process in coarsening [57].) However, almost 97% of 2289 sites of the lattice used in the simulations were twofold and threefold coordinated. Since the critical temperature for a one-dimensional chain of Potts spins is $T=0$, the transition temperature of this lattice is much smaller than T_c^{∞} (Ref. [58]). Our rough estimate of the transition temperature is $[0.5\pm 0.1]T_c^{\infty}$ (see Fig. 13). It follows that for $T\lesssim T_c^{\infty}$ a characteristic time of coarsening τ is no less than 1.6×10^7 MCS, far beyond our computational capabilities. This and other difficulties related to the boundary effects and described earlier did not allow us to verify whether the Gaussian curvature effects can be simulated by using a standard Potts model on an octagonal lattice. Obviously, the task would be much easier if an algorithm could be found that would implement periodic boundary conditions.

VI. CONCLUSIONS

We have proposed a model for grain coarsening on curved surfaces and investigated it by using Monte Carlo simulations. The model is an extension of a Potts model used in the past to study a variety of grain growth phenomena on flat surfaces [24–27,31–34]. In contrast to other, local models of coarsening, the presented model introduced a global field to simulate the dynamic effects due to the Gaussian curvature of the film.

As predicted by the recent theory of soap-froth kinetics on curved surfaces, we found that the stability properties of stationary grains are sensitive to the Gaussian curvature of the surface. In particular, it is found that on a spherical surface, no grain is stable. This is like abnor-

mal growth (secondary recrystallization) kinetics in planar systems. In a region of positive curvature, as on the surface of a sphere or on the outside of a torus, grains which are much larger than the mean grain size are unstable and grow faster than the mean and will engulf the entire surface section with $K>0$. In regions of negative curvature, as on the inside of a torus, all stationary grains are stable and the final configuration consists of many grains which have established a stable size, which is a decreasing function of $|K|$. A simple argument suggests that on the surface of a torus an abnormally large grain will penetrate the negatively curved regions covering up to 0.65... of the total surface. These observations are found to agree with results of experimental studies of the growth of grains in polycrystalline films on curved surfaces.

The usefulness of the suggested model is emphasized by inherent difficulties in the simulation of grain coarsening using a standard Potts model on lattices coresponding to regular tiling of surfaces with $K<0$, e.g., pseudosphere. Grain coarsening on an octagonal lattice with free boundary conditions yields microstructures with a mean grain size that reaches a constant value at large times. It is found, however, that the topology of the lattice results in the pinning of all triple vertices despite the fact that the stable domain shapes do not tile the surface of the pseudosphere. It is argued that for high enough temperatures and very long runs the curvature effects should be observed, if a lattice with periodic boundary conditions were used in the simulations.

ACKNOWLEDGMENTS

One of us (P.P.) wishes to thank M. J. Luton for his continued encouragement and assistance.

[1] D. Weaire and N. Rivier, Contemp. Phys. **25**, 59 (1984).
[2] H. V. Atkinson, Acta Metall. **37**, 469 (1988).
[3] J. A. Glazier and D. Weaire, J. Phys. Condens. Matter **4**, 1867 (1992).
[4] J. von Neumann, in *Metal Interfaces* (American Society for Metals, Cleveland, 1952), p. 108.
[5] W. W. Mullins, J. Appl. Phys. **27**, 900 (1956); **59**, 1341 (1988).
[6] N. Rivier and A. Lissowski, J. Phys. A **15**, L143 (1982).
[7] N. Rivier, Philos. Mag. B **47**, L45 (1983); **52**, 795 (1985).
[8] M. A. Peshkin, K. J. Strandburg, and N. Rivier, Phys. Rev. Lett. **67**, 1803 (1991).
[9] R. M. C. de Almeida and J. R. Iglesias, J. Phys. A **21**, 3365 (1988).
[10] M. Marder, Phys. Rev. B **36**, 438 (1987).
[11] C. W. J. Beenakker, Phys. Rev. Lett. **57**, 2454 (1987); Phys. Rev A **37**, 1697 (1988).
[12] I-Wei Chen, Acta Metall. **35**, 1723 (1987).
[13] J. Stavans, E. Domany, and D. Mukamel, Europhys. Lett. **62**, 1318 (1989).
[14] H. Flyvbjerg and C. Jeppesen, Phys. Scr. **T38**, 49 (1992).
[15] H. Flyvbjerg, Phys. Rev. E **47**, 4037 (1993).
[16] C. Godréche, I. Kostov, and I. Yekutieli, Phys. Rev. Lett. **69**, 2674 (1992).
[17] J. E. Avron and D. Levine, Phys. Rev. Lett. **69**, 208 (1992).
[18] J. Wejchert, D. Weaire, and J. P. Kermode, Philos. Mag. B **53**, 15 (1986).
[19] D. Weaire and J. P. Kermode, Philos. Mag. B **48**, 245 (1983); **50**, 379 (1984).
[20] J. Wejchert, D. Weaire, and J. P. Kermode, Philos. Mag. B **53**, 15 (1986).
[21] H. J. Frost and C. V. Thompson, Acta Metall. **35**, 289 (1987).
[22] K. Kawasaki, T. Nagai, and K. Nakashima, Philos. Mag. B **60**, 399 (1989).
[23] V. E. Fradkov, L. S. Shvindlerman, and D. G. Udler, Scripta Metall. **19**, 1285 (1985); V. E. Fradkov, A. S. Kravchenko, and L. S. Shvindlerman, *ibid.* **19**, 1291 (1985).
[24] M. P. Anderson, D. J. Srolovitz, G. S. Grest, and P. S. Sahni, Acta Metall. **32**, 783 (1984).
[25] D. J. Srolovitz, M. P. Anderson, P. S. Sahni, and G. S. Grest, Acta Metall. **32**, 793 (1984).
[26] D. J. Srolovitz, M. P. Anderson, G. S. Grest, and P. S. Sahni, Acta Metall. **32**, 1429 (1984).
[27] G. S. Grest, M. P. Anderson, and D. J. Srolovitz, Phys. Rev. B **38**, 4752 (1988).
[28] F. Bolton and D. Weaire, Phys. Rev. Lett. **65**, 3449 (1990); Philos. Mag. B **63**, 795 (1991); **65**, 473 (1992).
[29] D. Levine, J. E. Avron, and A. Brokman, Mater. Sci. Form. **94-96**, 281 (1992).
[30] P. Peczak (unpublished).
[31] M. P. Anderson, G. S. Grest, and D. J. Srolovitz, Philos. Mag. B **59**, 293 (1989).
[32] J. A. Glazier, M. P. Anderson, and G. S. Grest, Philos. Mag. B **62**, 615 (1990).
[33] E. A. Holm, J. A. Glazier, D. J. Srolovitz, and G. S. Grest, Phys. Rev. A **43**, 2662 (1991).
[34] F. Graner and J. A. Glazier, Phys. Rev. Lett. **69**, 2013 (1992).
[35] R. B. Potts, Proc. Camb. Philos. Soc. **48**, 106 (1952).
[36] J. E. Avron, H. van Beijeren, L. S. Schulman, and R. K. P. Zia, J. Phys. A **15**, L81 (1982).
[37] T. Hofsäss and H. Kleinert, J. Chem. Phys. **86**, 3565 (1987).
[38] M. P. de Carmo, *Differential Geometry of Curves and Surfaces* (Prentice-Hall, Englewood Cliffs, NJ, 1976).
[39] P. A. Firby and C. F. Gardiner, *Surface Topology* (Ellis Horwood, London, 1991).
[40] J. Viñals and J. D. Gunton, Phys. Rev. B **33**, 7795 (1986); **36**, 7036 (1987).
[41] An alternative method of dealing with occasional impingement of separate grains with the same orientation but different value of the Gaussian curvature field is to allow for an unobstructed growth which ultimately leads to the disappearance of one of these grains. An advantage of the adopted procedure is that it decreased the total time of coarsening by 10–20 % without significantly changing the final result of the simulations, which was confirmed in separate runs by using both methods.
[42] D. Kim and R. J. Joseph, J. Phys. C **7**, L167 (1974).
[43] M. S. S. Challa, D. P. Landau, and K. Binder, Phys. Rev. B **34**, 1841 (1986).
[44] J.-S. Ho and A. Baumgärtner, Mol. Simulation **6**, 163

(1991).
[45] D. J. Srolovitz, G. S. Grest, and M. P. Anderson, Acta Metall. **34**, 1833 (1986).
[46] D. J. Srolovitz, G. S. Grest, and M. P. Anderson, Acta Metall. **33**, 2233 (1985) and references therein.
[47] A. D. Rollett, D. J. Srolovitz, and M. P. Anderson, Acta Metall. **37**, 1227 (1989).
[48] O. Hunderi and N. Ryum, Acta Metall. **29**, 1737 (1981); **30**, 739 (1982).
[49] H. J. Frost, C. V. Thompson, and D. T. Walton, Acta Metall. Mater. **38**, 1445 (1990); **40**, 779 (1992).
[50] V. I. Smirnov, *A Course of Higher Mathematics* (Addison-Wesley, Reading, 1964), Vol. II, p. 367.
[51] D. Hilbert, Trans. Am. Math. Soc. **2**, 87 (1901).
[52] N. L. Balzas and A. Voros, Phys. Rep. **143**, 109 (1986).
[53] The critical temperature for the Q-state Potts model on a self-dual lattice does not depend on its coordination number and is given by $T_c^{\infty}=\ln^{-1}(1+Q^{-1/2})$, which is the well-known result for the square lattice [G. H. Wannier, Phys. Rev. **17**, 50 (1945)].
[54] P. S. Sahni, D. J. Srolovitz, G. S. Grest, M. P. Anderson, and S. A. Safran, Phys. Rev. B **28**, 2705 (1983).
[55] J. Viñals and M. Grant, Phys. Rev. B **36**, 7036 (1987).
[56] G. Grinstein and J. F. Fernandez, Phys. Rev. B **29**, 6389 (1984).
[57] J. D. Shore and J. P. Sethna, Phys. Rev. B **43**, 3782 (1991).
[58] It is worth noting that the algorithm that was used yields the octagonal lattice which has nearly all of its sites on the boundary. This leads to finite-size corrections to scaling which may have a very different form than their flat counterparts.